

Fig. 2. (a) Crater (50 km diameter) exhibiting a partial central peak ring offset uprange (from lower right) C1-60N 263. Radar look direction is from upper left. (b) Larger crater (103 km diameter) exhibiting central peak ring offset downrange from present rim, opposite to occurrence in (a) and Fig. 1. Reversal in position is related to enhanced rim/wall collapse uprange that widens and circularizes the crater around the deepest portion of the transient crater cavity, which occurs uprange. Further crater widening follows pre-existing structural grain. C1-30N 135.

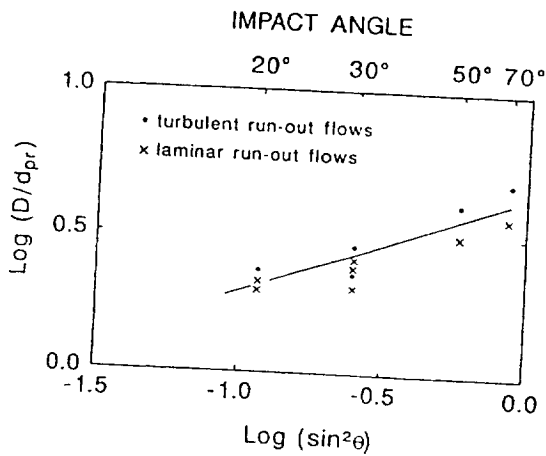


Fig. 3. Effect of impact angle (from horizontal) on the transverse diameter of the central peak ring d_{cp} referenced to crater diameter. As impact angle decreases (based on degree of ejecta symmetry), size of central peak ring becomes larger relative to crater diameter. Such a trend is expected if central peak ring reflects the size of impactor and cratering efficiency decreases impact angle.

The enhanced uprange rim/wall collapse illustrated in Fig. 2b (and numerous other large oblique impacts on Venus) provides insight for why most craters exhibit a circular outline even though early-time energy transfer comprises a larger fraction of crater growth. Failure of the uprange rim/wall in response to the oversteepened wall and greater floor depth circularizes crater outlines. The rectilinear and conjugate scarp on the pattern uprange rim, however, indicates failure along preimpact stresses. Hence, a corollary is that peak shock levels and particle motion may be reduced uprange during oblique impacts due to the downrange motion of the impactor, analogous to time dilation.

References: [1] Gault D. E. and Wedekind J. A. (1978) *Proc. LPSC 9th*, 3843-3875. [2] Moore H. J. (1979) *U.S. Geol. Surv. Prof. Pap.* 812-13, 47 pp. [3] Gault D. E. and Wedekind J. A. (1977) In *Impact and Explosion Cratering* (D. Roddy et al., eds.), 1231-1244, Pergamon, New York. [4] Holsapple K. A. and Schmidt R. M. (1987) *JGR*, 92, 6350-6376. [5] Schultz P. H. and Gault D. E. (1991) *Meteoritics*, 26. [6] Wichman R. W. and Schultz P. H. (1992) *LPSC XXIII*, 1521-1522. [7] Schultz P. H. (1988) In *Mercury* (F. Vilas et al., eds.), 274-335, Univ. of Arizona, Tucson. [8] Schultz P. H. (1992) *JGR*, in press.

N93-14372 084370
IMPACT-GENERATED WINDS ON VENUS: CAUSES AND EFFECTS. Peter H. Schultz, Brown University, Department of Geological Sciences, Box 1846, Providence RI 02912, USA.

The pressure of the dense atmosphere of Venus significantly changes the appearance of ejecta deposits relative to craters on the Moon and Mercury. Conversely, specific styles and sequences of ejecta emplacement can be inferred to represent different intensities of atmospheric response winds acting over different timescales. Three characteristic timescales can be inferred from the geologic record: surface scouring and impactor-controlled (angle and direction) initiation of the long fluidized run-out flows; nonballistic emplacement of inner, radar-bright ejecta facies and radar-dark outer facies; and very late reworking of surface materials. These three timescales roughly correspond to processes observed in laboratory experiments that can be scaled to conditions on Venus (with appropriate assumptions): coupling between the atmosphere and early-time vapor/melt (target and impactor) that produces an intense shock that subsequently evolves into blast/response winds; less energetic dynamic response of the atmosphere to the outward-moving ballistic ejecta curtain that generates nonthermal turbulent eddies; and late recovery of the atmosphere to impact-generated thermal and pressure gradients expressed as low-energy but long-lived winds. These different timescales and processes can be viewed as the atmosphere equivalent of shock melting, material motion, and far-field seismic response in the target.

Early Processes (Direct Effects of Blast and Fireball): Under vacuum conditions, the fate of the impactor is generally lost; even on the Earth, most impact melt sheets exhibit little trace of the impactor. The dense atmosphere of Venus, however, prevents escape of the impactor through rapid deceleration of ricochet debris and containment of the vapor cloud [1,2]. Figure 1a illustrates the time required for the atmospheric blast front to decelerate to the speed of sound as a function of crater size, where k is the fraction the initial impactor energy (KE_i) coupled to the atmosphere (E_A). On Venus, the shock front dissipates before the crater finishes forming. If the blast is created by deceleration and containment of early high-speed ejecta (downrange jetting and ricochet/vapor), then it will precede ejecta emplacement and should exhibit a source area offset

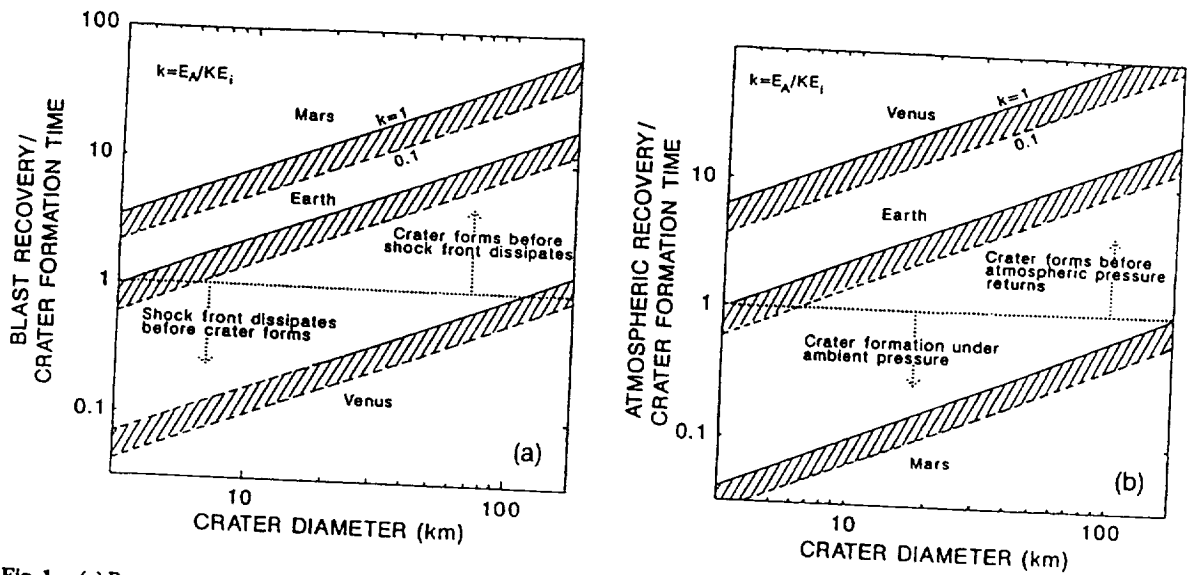


Fig. 1. (a) Recovery time for atmospheric blast to reduce to the speed of sound on Venus scaled to crater formation time. The value of k represents the fraction of initial impactor kinetic energy (KE_i) coupled to the atmosphere (E_A). On Venus the blast effects should precede crater formation time. Although atmospheric pressure has recovered, high temperatures (the fireball) result in low densities. Thermal gradients and motion of fireball induce strong recovery winds that rework ejecta at late times. (b) Recovery time for atmospheric pressure behind the shock front to return to ambient conditions on Venus scaled to crater formation time. Although atmospheric pressure has recovered, high temperatures (the fireball) result in low densities. Thermal gradients and motion of fireball induce strong recovery winds that rework ejecta at late times.

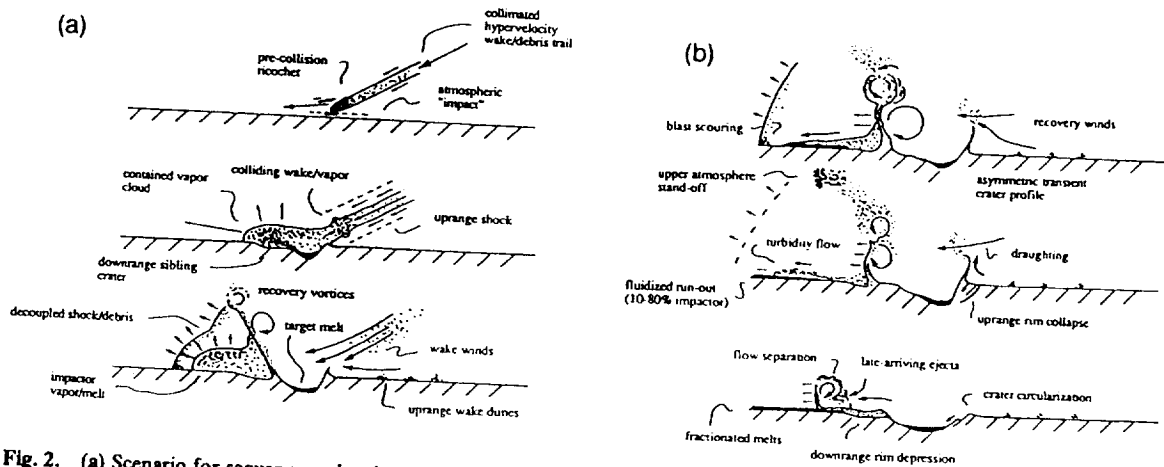


Fig. 2. (a) Scenario for sequence and style of ejecta emplacement at early times based on inferences drawn from laboratory impact phenomena scaled to Venus and surface features revealed by Magellan. At early times, kinetic energy and momentum in the vapor cloud evolves into a downrange-moving fireball that creates strong winds downrange. (b) Scenario for late processes. Winds and turbulence created by the outward-moving ejecta curtain entrain coarse fractions to produce an avalanchelike flow of coarse inner ejecta deposits. Such deposits persist as radar-bright ejecta deposits because of the roughness and low ambient surface winds. Finer fractions entrained in sustained turbulence result in turbidity flows with potentially much greater run-out distances. Deposits from these flows will be more susceptible to subsequent erosion.

downrange from the crater [2,3]. The downrange offset of the center of origin of the shock is observed in laboratory impact experiments. Features consistent with this interpretation can also be found around venusian craters and include [2] topographic barriers shadowing surface disruption from the blast; radar-dark/-bright striations converging on the downrange rim rather than the crater; and diffuse haloes at the base of small hills again focusing on a downrange rim "source" (shock-dislodged debris drawn back into the rarefied, rising fireball). Moreover, radar-dark parabola patterns commonly center on a point downrange and not the crater [2]. In contrast, the time for recovery of the atmosphere to ambient pressure (or density and temperature) is much longer than the time for crater formation

(Fig. 1b). If all craters were formed by vertical impacts, this would mean that the craters form within a fireball or behind the wake characterized by low density (high temperature, low pressure) as postulated in [4]. But most craters are formed by oblique impacts (i.e., 75% formed at angles of 60° or less). Consequently, the early fireball moves away from crater excavation initially at hypervelocities. At low impact angles (<30°), the energy coupled to the atmosphere resembles a rolling fireball containing vapor and dispersed melt moving downrange until decelerated. Because the vapor/melt is higher in density than conditions in the fireball, it collapses within the fireball to form long run-out density flows controlled by local topography, well in advance of ejecta emplace-

ment as observed on Venus [5,6]. Such a process accounts for the long run-out flows consistently originating downrange in oblique impacts (i.e., opposite the missing ejecta sector) even if uphill from the crater rim. Atmospheric turbulence and recovery winds decoupled from the gradient-controlled basal run-out flow continues downrange and produces wind streaks in the lee of topographic highs. Turbulence accompanying the basal density flows may also produce wind streak patterns. Uprange the atmosphere is drawn in behind the fireball (and enhanced by the impinging impactor wake), resulting in strong winds that will last at least as long as the time for crater formation (i.e., minutes). Such winds can entrain and saltate surface materials as observed in laboratory experiments [2,3] and inferred from large transverse dunes uprange on Venus [2].

Atmospheric Effects on Ballistic Ejecta: Even on Venus, target debris will be ballistically ejected and form a conical ejecta curtain until its outward advance is decelerated by the atmosphere. The well-defined, radial ejecta delineating the uprange missing ejecta sector of craters formed by oblique impacts demonstrate ballistic control of ejection. As the inclined ejecta curtain advances outward, however, it creates turbulent vortices, which have been observed in the laboratory experiments [2] and modeled theoretically [7]. The ejecta curtain gradually becomes more vertical in response to atmospheric resistance. The atmospheric density is sufficient to decelerate meter-sized ejecta to terminal velocities [8] that will be entrained in and driven by response winds induced by the outward-moving curtain. While larger ejecta are deposited, smaller size fractions become entrained in an outward ejecta flow. Based on diversion of such flows by low-relief barriers near the rims of craters, the transition from ballistic to nonballistic emplacement occurs within about 0.5 crater radii of the rim. This observation underscores the fact that dynamic atmospheric pressure significantly restricts outward advance of the ejecta curtain. The scaled run-out distance (distance from the crater rim scaled to crater diameter, D) of the ejecta flow should decrease on Venus as $D^{-0.5}$, unless consumed by crater rim collapse. Because of the high atmospheric density, collapse of near-rim ejecta into a flow crudely resembles an avalanche comprised of coarse debris and blocks. But high winds and turbulence created by the outward-moving curtain separate during terminal emplacement of the inner flow, thereby winnowing the finer fractions and creating an overrunning turbidity flow that continues outward.

Turbidity flows containing finer fractions can extend to much larger distances until turbulence supporting entrained debris no longer can support the load. Because turbulent wind velocities greatly exceed ambient surface winds, such vortices are also capable of mobilizing surface materials. It is suggested that the radar-dark lobes extending beyond the inner radar-bright ejecta [2,6] reflect this process. In addition, many craters are surrounded by a very diffuse boundary that masks low-relief ridges and fractures; this boundary may indicate the limits of a third stage of flow separation and deposition. The observed radar-dark signature requires such ejecta to be less than a few centimeters. In contrast with the coarse, radar-bright inner facies, the outer radar-dark facies will be more susceptible to later erosion by ambient or other impact-generated winds because the size fractions were sorted by a similar process. This is consistent with observed removal or reworking of craters believed to be old, based on superposed tectonic features.

Late Recovery Winds (Secondary Effects of Atmospheric Turbulence): On planets without atmospheres, the effects of early, high-speed ejecta and impactor are typically lost. On Venus, however, the dense atmosphere not only contains this energy fraction, but the long recovery time of the atmosphere (Fig. 1b)

results in late-stage reworking, if not self-destruction, of ejecta facies emplaced earlier. Surface expression should include bedforms (e.g., meter-scale dunes and decimeter-scale ripples) reflecting eddies created in the boundary layer at the surface. Because radar imaging indicates small-scale surface roughness (as well as resolved surface features), regions affected by such long-lived low-energy processes can extend to enormous distances. Such areas are not directly related to ejecta emplacement but reflect the atmospheric equivalent to distant seismic waves in the target. Late-stage atmospheric processes also include interactions with upper-level winds. Deflection of the winds around the advancing/expanding fireball creates a parabolic-shaped interface aloft. This is preserved in the fall-out of finer debris for impacts directed into the winds aloft (from the west) but self-destructs if the impact is directed with the wind. Exception to this rule occurs for larger crater (>60 km) sufficient to interrupt the flow pattern not only by the fireball but also by the ejecta curtain.

References: [1] Schultz P. H. and Gault D. E. (1990) In *GSA Spec. Pap.* 247 (V. L. Sharpton and P. D. Ward, eds.), 239–261. [2] Schultz P. H. (1992) *JGR*, in press. [3] Schultz P. H. (1992) *JGR*, in press. [4] Ivanov B. A. et al. (1986) *Proc. LPSC 16th*, in *JGR*, 91, D413–D430. [5] Schultz P. H. (1991) *Eos*, 73, 288. [6] Phillips R. J. et al. (1991) *Science*, 252, 288–296. [7] Barnouin O. and Schultz P. H. (1992) *LPSC XXIII*, 65–66. [8] Schultz P. H. and Gault D. E. (1979) *JGR*, 84, 7669–7687. [9] Schultz P. H. et al. (1981) In *Multi-Ring Basins, Proc. LPS 12A* (P. H. Schultz et al., eds.), 181–195, Pergamon, New York. [10] Barnouin O. and Schultz P. H. (1992) *LPSC XXIII*, 65–66. [11] Schultz P. H., this volume. [12] Jones E. M. and Sanford M. T. II (1982) In *GSA Spec. Pap.* 190 (L. Silver and P. Schultz, eds.), 175–186. [13] Schultz P. H. (1992) *JGR*, in press. [14] Schultz P. H. and Gault D. E. (1982) In *GSA Spec. Pap.* 190 (L. Silver and P. Schultz, eds.), 153–174. [15] Post R. L. (1974) *AFWL-TR-74-51*.

N93-14373

MAGELLAN PROJECT PROGRESS REPORT. J. F. Scott, D. G. Griffith, J. M. Gunn, R. G. Piereson, J. M. Stewart, A. M. Tavormina, and T. W. Thompson, Jet Propulsion Laboratory, California Institute of Technology, Pasadena CA 91109, USA.

The Magellan spacecraft was placed into orbit around Venus on August 10, 1990 and started radar data acquisition on September 15, 1990. Since then, Magellan has completed mapping over 2.75 rotations of the planet (as of mid-July 1992). Synthetic aperture radar (SAR), altimetry, and radiometry observations have covered 84% of the surface during the first mission cycle from mid-September 1990 through mid-May 1991.

Operations in the second mission cycle from mid-May 1991 through mid-January 1992 emphasized filling the larger gaps (the south polar region and a superior conjunction) from that first cycle. An Orbit Trim Maneuver (OTM) was performed at the beginning of cycle 2 in order to interleave altimeter footprints at periapsis. This yielded better altimetric sampling of the equatorial regions of Venus. Some 94% of the planet was mapped at the end of mission cycle 2.

Observations in the third mission cycle from mid-January to mid-September 1992 emphasized reimaging of areas covered in cycle 1 and cycle 2 such that digital stereo and digital terrain data products can be produced. A transponder anomaly in January 1992 (just before mission cycle 3 started) forced the project to use a radar data downlink of 115 Kbs instead of 268 Kbs. Although data acquisition is curtailed, some 30–40% of the planet will be mapped